# HOHLRAUM ENERGETICS WITH SMOOTH LASER BEAMS


*S. H. Glenzer* *B. A. Hammel* *M.-C. Monteil** *G. F. Stone*

*R. L. Berger* *R. L. Kauffman* *J. D. Moody* *L. J. Suter*

*M. A. Blain** *R. K. Kirkwood* *T. J. Orzechowski* *R. E. Turner*

*S. N. Dixit* *O. L. Landen* *D. M. Pennington* *T. L. Weiland*

*K. G. Estabrook* *B. J. MacGowan*


## Introduction

The controlled and efficient coupling of laser or ion-beam energy to a fusion target is a key issue in inertial confinement fusion research. In the indirect-drive approach,[1,2] current ignition designs for the National Ignition Facility (NIF) use high-$Z$ hohlraums as radiation enclosures that are heated with shaped, high-power laser beams with more than 1-MJ energy. At the inner wall of the hohlraum, the heater beam power is converted into soft x rays characterized by a radiation temperature $T_{rad}$ (Refs. 3–6). The x rays drive the implosion of the fusion capsule by x-ray ablation pressure. Integrated radiation-hydrodynamic LASNEX simulations of both the hohlraum and capsule conditions show a significant fusion yield of 16 MJ when using hohlraums filled with a low-$Z$ gas.[2,7,8] The gas inhibits movements of the laser absorption and x-ray emission region and prevents early axial stagnation of the high-$Z$ plasma blowoff. These are important properties of gas-filled hohlraums for maintaining radiation symmetry and a symmetric, high-convergence, high-yield implosion of the fusion capsule.

We present complementary measurements of radiation temperatures and stimulated scattering losses arising from stimulated Brillouin scattering (SBS) and stimulated Raman scattering (SRS)[9,10] from laser-driven, ignition-type hohlraums. We show that the x-ray production in gas-filled hohlraums is reasonably well described by radiation-hydrodynamic LASNEX[11,12] modeling and by scaling laws[13] when taking into account the scattering losses. The experiments further show that laser-beam smoothing techniques are successful for the controlled and efficient production of ignition-relevant hohlraum plasmas. This result was obtained with two different laser pulse shapes. One resulted in laser intensities of $2 \times 10^{15}$ W/cm$^2$ to study hohlraums heated with the same intensities as those planned for the NIF. In addition, hohlraum conditions were investigated with a second laser pulse shape with higher intensities, reaching $4 \times 10^{15}$ W/cm$^2$, to investigate scalings and the physics of high-temperature hohlraums.

In this study, we demonstrate that SBS and SRS losses from hohlraums heated with intensities of $2 \times 10^{15}$ W/cm$^2$ can be controlled and reduced to the 3% level by applying laser-beam smoothing techniques. For higher heater-beam intensities of $4 \times 10^{15}$ W/cm$^2$, the best smoothing condition resulted in a maximum loss of 7%. These findings are consistent with experimental observations and calculations showing that filamentation and gain for SBS and SRS are reduced in hohlraum plasmas by the suppression of hot spots in the smoothed laser beams. In the $2 \times 10^{15}$ W/cm$^2$ case, the radiation temperature increases by ~15 eV, showing clear evidence of improved laser–energy coupling into the hohlraum. Table 1 identifies the acronyms used in this article.

TABLE 1. List of acronyms and definitions.

| | |
|---|---|
| FABS | full-aperture backscattering diagnostic |
| KPP | kinoform phase plate |
| LEH | laser entrance hole |
| NBI | near-backscattering imager |
| NIF | National Ignition Facility |
| PCD | photoconductive detector |
| PS22 | pulse shape number 22: 7-TW foot to 17-TW peak power, total energy ≈ 29 kJ (see Figure 6b) |
| PS26 | pulse shape number 26: 5-TW foot to 25-TW peak power, total energy ≈ 31 kJ (see Figure 7c) |
| RPP | random phase plate |
| SBS | stimulated Brillouin scattering |
| SRS | stimulated Raman scattering |
| SSD | smoothing by spectral dispersion |


*Centre D'Etudes de Limeil-Valenton, Villeneuve Saint-Georges, France

# Experiment

The experiments were performed at the Nova laser facility at Lawrence Livermore National Laboratory.[14] As shown in Figure 1, we used cylindrical hohlraums that were 2.75 mm long and 1.6 mm in diameter, the standard size for capsule implosions[15,16] and current benchmarking experiments[17–19] at Nova. On each side, five laser beams enter the hohlraum through laser entrance holes (LEHs). In addition to empty hohlraums, we shot hohlraums filled with 1 atm of methane ($CH_4$) and used 0.35-$\mu$m-thick polyimide to cover holes. The hohlraums were heated with a total of ten shaped laser beams of 2.4-ns duration. The pulses rose from a 7-TW foot to 17-TW peak power (pulse shape number 22, hereafter PS22) or from 5 TW to 25 TW (pulse shape number 26, PS26). Total energies supplied to the target were 29 kJ and 31 kJ, respectively.

Experiments were performed with standard, unsmoothed Nova beams and with two types of beam-smoothing conditions. The beams were smoothed by using kinoform phase plates (KPPs),[20,21] which break each beam into many several-millimeter-scale beamlets. The diffraction-limited focal spots are then superposed in the target plane, producing an intensity envelope without large scale-length inhomogeneities, but consisting of fine-scale hot spots (speckles). The focal spot was further smoothed through the use of smoothing by spectral dispersion (SSD).[22] In essence, the bandwidth of 0.22 nm at 1ω, together with a dispersive grating in the beamline, serves to move the speckles in the focal plane on time scales (~5 ps) that are short compared with that required for hot spots to form a filament in the plasma (~10 to 20 ps). The configuration resulted in peak laser intensities of 2 to $4 \times 10^{15}$ W/cm$^2$ at the LEHs, values that are comparable to those anticipated in NIF hohlraums (namely, $2 \times 10^{15}$ W/cm$^2$).

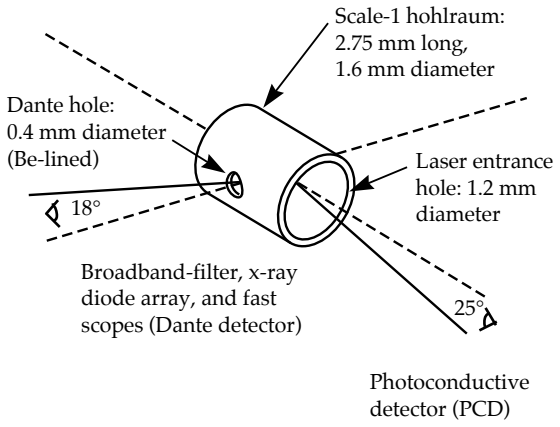


FIGURE 1. Schematic of a hohlraum target showing the views of the detectors. (08-00-0598-1178pb01)

Radiation temperatures were measured with a broadband-filter, x-ray diode array, and fast scopes (Dante detector).[23] This instrument measures the radiation flux per steradian, temporally and spectrally resolved $\phi(t,\nu)$, emitted along the collimated line of sight from the indirectly heated wall opposite a 450-$\mu$m-diam diagnostic hole in the side of the hohlraum (see Figure 1). We obtained the hohlraum wall temperature by

$$\nu(t) = \sigma[T_{\text{wall}}(t)]^4 A_{\text{d}}\,, \tag{1}$$

where $\nu(t)$ is the frequency-integrated radiation flux (0 to 2 keV) emitted from the wall through a diagnostic hole (area $A_{\text{d}}$), and $\sigma$ is the Stefan–Boltzmann constant. Closure effects of the diagnostic hole at late times were mitigated using a Be-lined hole. In addition to Dante measurements, we fielded a photoconductive detector (PCD)[24] on the PS26 experiments, which provided a radiation-temperature measurement through the 1.2-mm-diam LEH at a polar angle of 25°, for which closure effects are less important.[25]

We used three independent detection systems for a complete measurement of the scattering losses. Backscattering into the lens of one of the Nova laser beams was detected with a full-aperture backscattering diagnostic (FABS).[26] The light was imaged onto a frosted silica plate and detected temporally and spectrally resolved. For this purpose, we used properly filtered diodes with a temporal resolution of up to ~100 ps, a 0.25-m spectrometer for SRS, and a 0.75-m spectrometer for SBS. The spectrometers were equipped with optical streak cameras, resulting in a temporal resolution of ~30 ps. The entire detection system was absolutely calibrated in situ by retroreflecting 8% of a full-power laser shot into the detector. Light scattered at larger angles, up to 22°, was measured with a near-backscattering imager (NBI)[27]. This device consisted of a calibrated Al scatter plate mounted around the lens and 2D imaging detectors for SBS and SRS. Light scattered at larger angles was collected with calibrated diodes.

# Experimental Results and Discussion

Figure 2 compares experimental wall temperatures from Dante and time-integrated SBS and SRS losses of $CH_4$-filled and empty hohlraums for various beam-smoothing conditions. Data is shown for the PS22 experiments only because no measurements were performed for PS26 without laser-beam smoothing. We observe a clear correlation of these quantities. For gas-filled hohlraums, the total scattering losses are reduced from 18% ± 3% for unsmoothed laser beams to 3% ± 1% when applying KPPs plus 0.22-nm SSD.

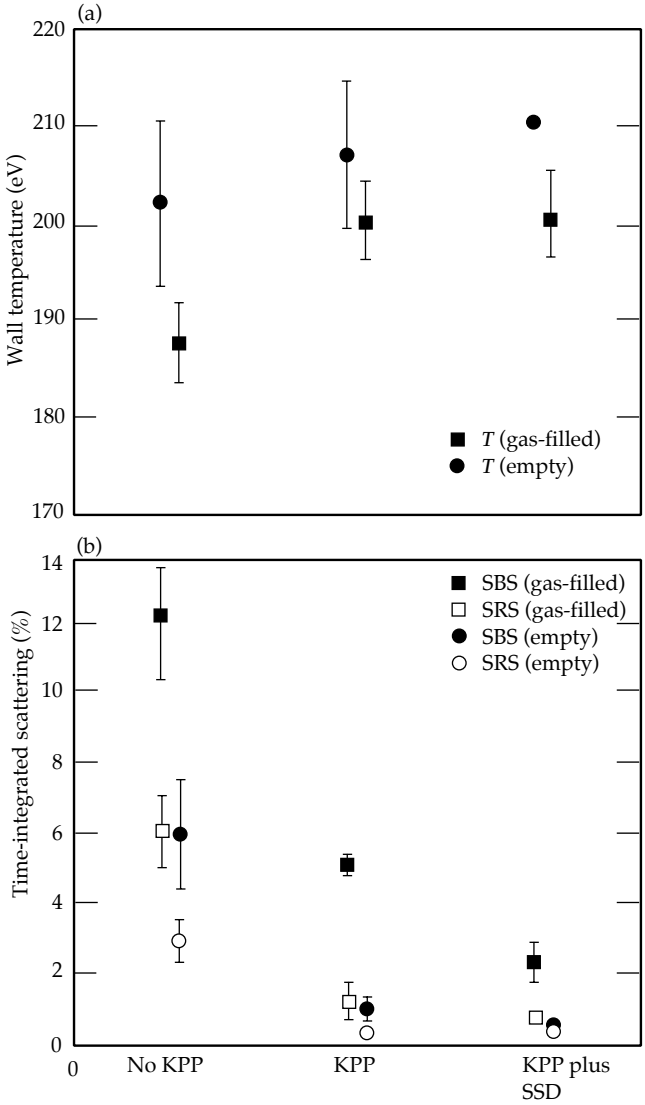


FIGURE 2. (a) Peak hohlraum wall temperatures for various laser-beam smoothing conditions. Error bars are rms values. (b) Time-integrated stimulated Brillouin and Raman scattering losses for gas-filled and empty hohlraums. Total energy loss for gas-filled hohlraums decreases from 18% for unsmoothed beams to 4% for beams smoothed with KPP plus SSD. For empty hohlraums, the reduction is from 9 to 1%. (08-00-0598-1180pb01)

Simultaneously, the temperatures increase by 15 eV. These results were found to be insensitive to variations in laser-beam focusing or to the laser power during the low-intensity foot. For hohlraums heated with smoothed laser beams, LASNEX simulations[25] show that the Dante-measured radiation temperatures may be 5 eV higher than those for unsmoothed beams merely due to suppression of laser-beam deflection.[28,29] This result is expected because unsmoothed Nova beams are deflected away from the midplane of the hohlraum, where wall temperatures are measured. The additional 10-eV increase in hohlraum temperatures observed in this study for smoothed laser beams is consistent with the reduction of backscatter losses, and it is clear evidence of improved energy coupling into the hohlraum.

Our scattering measurements indicate that filamentation of the laser beams is suppressed when applying beam smoothing, thus explaining the low scattering losses in the present experiments. Figure 3 shows SRS spectra at 1.8 ns $< t <$ 2 ns for the various smoothing conditions. The long-wavelength Raman feature at 550 nm plasma originates from plasma regions with $T_e = 3$ keV, $n_e = 7 \times 10^{20}/\text{cm}^3$. Using LASNEX simulations of the low-density plasma, which have been benchmarked against Thomson scattering measurements,[19] we find that the scattering at 550 nm arises from the CH plasma in the LEH region of the hohlraum. The width of 30 nm for the best smoothing condition (KPP plus SSD) is consistent with calculations of the damping and growth rate of electron plasma waves using the experimental parameters ($T_e = 3$ keV, $n_e = 7 \times 10^{20}/\text{cm}^3$, $\theta = 180°$ angle of observation, $2 \times 10^{15}$ W/cm$^2$, and $\lambda_0 = 351.1$ nm) in addition to estimates for the length of the interaction using simulated density gradients. The Raman signal at shorter wavelengths, 400 nm $< \lambda <$ 530 nm, originates from plasma regions with much lower densities (1 to 7% $n_{cr}$) than the average density of the methane plasma. The appearance of SRS from such low densities can be interpreted as an indication of filamentation of the laser beams.[26] The short-wavelength Raman signal is gradually suppressed with improved beam smoothing because of the reduction of energy in hot spots, which produce filamentation (KPP only), and the reduction of the filamentation rate of hot spots (with additional SSD).

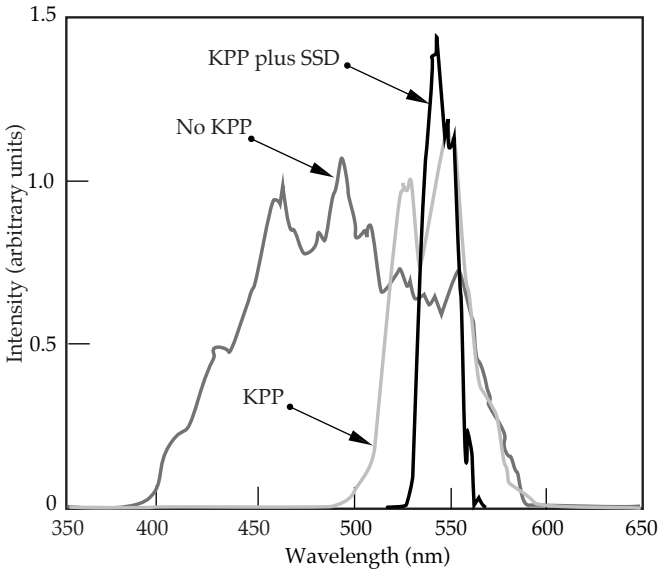


FIGURE 3. SRS spectra from gas-filled hohlraums at 1.8 ns $< t <$ 2 ns for various smoothing conditions. With improved smoothing, the spectra narrow from 180 to 30 nm. (08-00-0598-1182pb01)

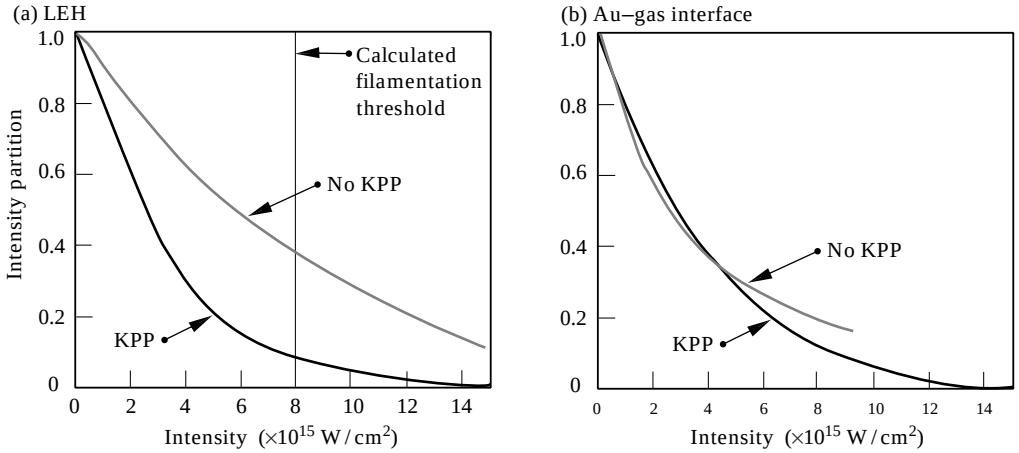


FIGURE 4. Intensity distribution in the laser beams (a) at the LEH and (b) at the Au–gas interface. At the LEH, more than 30% of an unsmoothed Nova beam exceeds the filamentation threshold. For a KPP-smoothed beam, only ~5% is above that threshold. This comparison is less favorable at the Au–gas interface. (08-00-0598-1183pb01)

These experimental observations are consistent with calculations of the filamentation threshold.[30–32] For our plasma conditions, they show that the laser beams filament for intensities of $I > 5$ to $8 \times 10^{15}$ W/cm$^2$. For unsmoothed laser beams, more than 30% of the laser beam exceeds this threshold in the LEH region, where Raman scattering occurs (see Figure 4a). On the other hand, a smoothed laser beam shows a significantly smaller fraction of high-intensity spots. Typically less than 5% of a Nova beam smoothed with a KPP is above the filamentation threshold; therefore, such beams are more stable against filamentation.

The favorable intensity distribution in the KPP-smoothed laser beams at the LEH explains the reduction of SRS losses by a factor of 6. Figure 4a shows the intensity distribution in the beam at the LEH, and Figure 4b shows the intensity distribution at the Au–gas interface. Absorption of the laser beam is neglected in these calculations. The intensity distribution in the beam at the LEH is more favorable than at the Au–gas interface, where calculations show the highest gain for SBS. Therefore, we expect a smaller reduction of SBS losses when applying beam smoothing. This picture is consistent with a reduction of the SBS losses by only a factor of 2 when applying KPP smoothing as observed in the experiment (Figure 2b).

F3D simulations of filamentation and SBS in flowing Au plasma have shown that the SBS with random phase plate (RPP) or KPP illumination is reduced modestly when SSD is added. The simulations are about 50 ps long and use plasma parameters deduced from LASNEX and an average laser intensity of $3 \times 10^{15}$ W/cm$^2$. The simulation assumes that the interaction occurs near the focal plane of an $f/4$ optic such that the hot-spot structure has the characteristic size of $f/4$ speckles and a speckle intensity distribution $P(I) = [\exp(I/I_0)]/(I_0)$. The length of the Au region, 210 $\mu$m, is similar to the LASNEX simulations (with an axial flow gradient that limits the gain of SBS), but the transverse size of the simulation region is much smaller than the laser beam spot size. The reduction is similar to that observed in the experiments and is associated with the control of hot-spot self-focusing.

The suppression of filamentation in the low-$Z$ plasma for smoothed beams is also consistent with the spatially resolved measurements of the SBS signal.

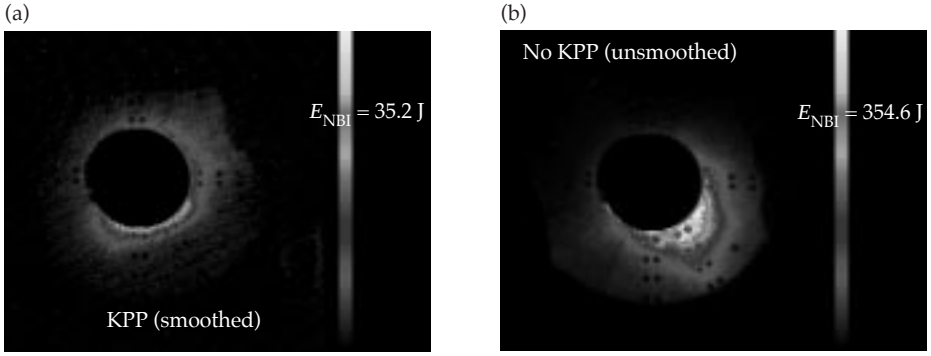


| | No KPP | KPP |
|---|---|---|
| % in lens | 40 | 85 |
| angle | 8° | 2° |

FIGURE 5. Spatial dependence of the Brillouin backscattered light from gas-filled hohlraums. Data is shown (a) for a KPP-smoothed beam and (b) for an unsmoothed beam. SBS from a KPP-smoothed beam is directed almost straight back into the lens, whereas the centroid of an unsmoothed beam is shifted 8° downward. (08-00-0598-1185pb01)

Figure 5 shows the backscattered SBS light observed with the NBI detector. For smoothed laser beams (Figure 5a) the Brillouin signal is scattered back almost straight into the lens (which is represented by the black, circular surface in the center of the image). Only a small spatial shift of the backscattered light of 2° ± 1° can be seen. On the other hand, unsmoothed laser beams show a backscattered Brillouin signal that is spatially shifted by up to 8° ± 1° away from the straight-backward direction (Figure 5b).

These observations can be interpreted in the following way. As laser beams traverse the low-density plasma on their way to the hohlraum wall, they filament in the low-Z plasma in the LEH region and are deflected towards the LEH. SBS occurs when the beam reaches the high-Z Au plasma of the hohlraum wall and is scattered back, but will not retrace the incoming path, resulting in a spatial shift of the SBS signal as observed with the NBI detector. This interpretation is consistent with so-called spot motion experiments[18,33] and with calculations[34] for unsmoothed laser beams. The experiments described by Delamater et al.[18] and Kauffman et al.[33] show a deflection of laser beams toward the LEHs, which was greatly reduced when beam-smoothing techniques were applied. The calculations by Hinkel et al.[34] show a deflection of unsmoothed laser beams by about 6° for parameters similar to those in this study. Those results are in reasonable agreement with the observation in Figure 5.

For unsmoothed beams, our measurements with the FABS and the NBI show that 40% of the SBS light is scattered straight back into the lens, and 60% is scattered at larger angles. The light is mostly scattered in the downward direction, which is consistent with a deflection of the incoming laser beam toward the LEH. For smoothed beams, on the other hand, more than 85% of the light is scattered straight back into the lens, indicating that beam deflection is effectively suppressed.

Figure 6a compares the measured and calculated hohlraum wall temperatures as a function of time for a PS22 experiment. The calculations use corrected pulse shapes; i.e., scattering losses due to SBS and SRS were subtracted to obtain the laser power absorbed in the hohlraum, as shown in Figure 6b. Some discrepancies between the measured and calculated temperatures can be seen during the low-intensity foot with $t > t_0 + 1$ ns, and at the end of the hohlraum heating for $t > t_0 + 2$ ns. In the first case, we typically observe that the LASNEX simulations underestimate the temperatures by 10 to 15 eV. We observe this discrepancy when using higher laser intensities during the foot of the pulse, as in the PS22 experiments. A model was developed[12] that accounts for this underestimation. The model postulates that energy is transported directly to the hohlraum wall, seen by the Dante detector, due to laser sidescattering or electron transport. The result is a larger wall temperature than

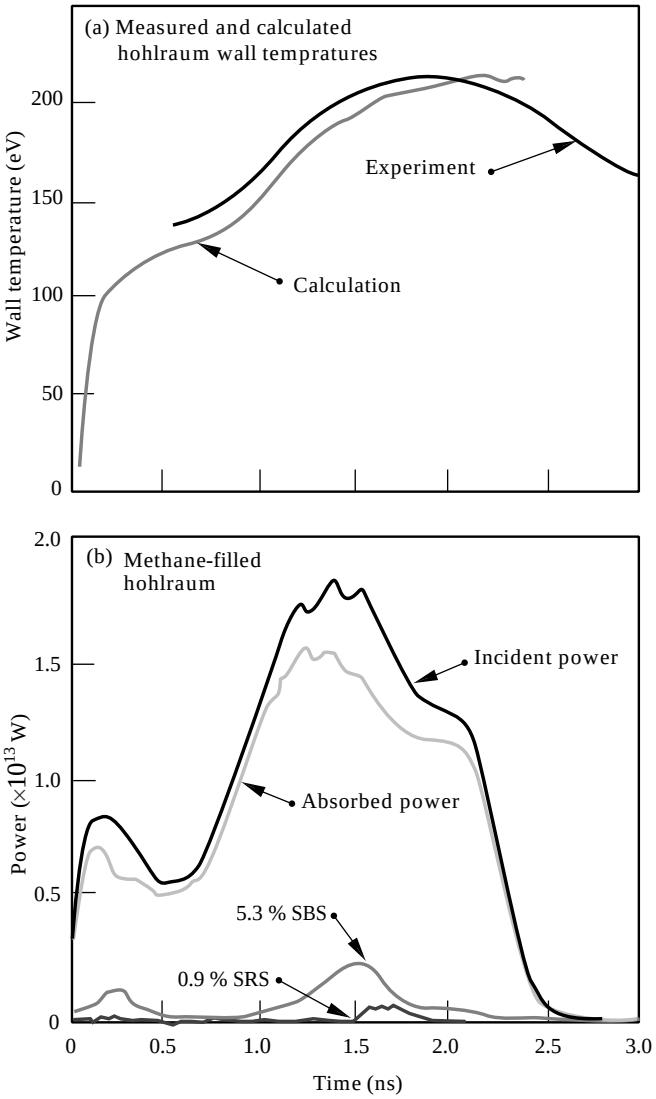


FIGURE 6. (a) Experimental hohlraum-wall temperature for a gas-filled hohlraum heated with PS22 (not albedo corrected) as a function of time from the Dante detector. (b) Laser power with scattering losses as function of time. (08-00-0598-1186pb01)

that calculated. This model has not yet been confirmed experimentally. However, in ignition experiments, radiation temperature in the foot can be readily adjusted to provide appropriate initial shocks for the implosion of the fusion capsule by reducing the laser power during the foot. The LASNEX calculations agree well with the peak temperature seen with Dante.

The LASNEX simulations of x-ray flux were post-processed to match the viewing angle of both detectors. In addition, calculations were performed to estimate the effect of the Be-lined Dante "washer" on the modeled temperatures. The liner can affect the hohlraum temperature both by absorbing radiation and by injecting low-Z material into the hohlraum. We cannot model the structure directly because it is a 3D

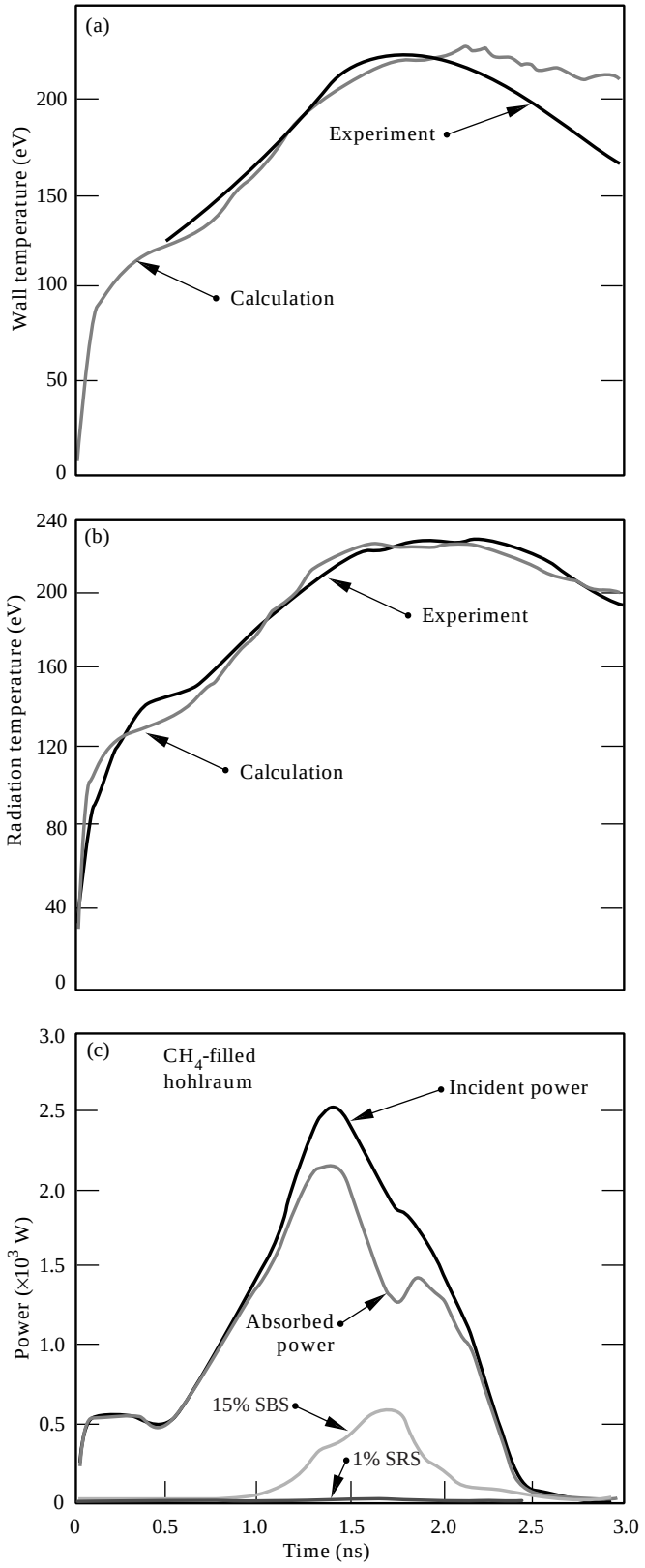


FIGURE 7. (a) Experimental hohlraum-wall temperature for a gas-filled hohlraum heated with PS26 (not albedo corrected) from the Dante detector, and (b) radiation temperature from the PCD. (c) Laser power with scattering losses as function of time. (08-00-0598-1189pb01)

feature on the side of the hohlraum. However, we can attempt to approximate its effect through simulations that include a Be sphere in the center of the numerical hohlraum that has the same area as the Be washer. During the period of peak drive, these simulations result in a temperature that averages approximately 3 eV cooler (not shown) than simulations without the Be sphere.

Figure 7a shows the measured hohlraum-wall temperature as a function of time for an experiment with PS26. The measurements of radiation temperature compare well to the results for detailed radiation hydrodynamic modeling. In particular, at the peak of the x-ray drive at $t > t_0 + 1.8$ ns, the measured and calculated temperatures match well. Once again, the calculations use corrected pulse shapes with SBS and SRS losses subtracted (see Figure c). To estimate the hohlraum radiation temperature $T_{rad}$ for the purpose of simulating capsule implosion dynamics, we must include the fact that the capsule is irradiated by x rays from both the indirectly and directly heated hohlraum wall. To infer $T_{rad}$, we use the time-dependent albedo $\alpha(t)$, which is the ratio of the re-emitted flux over the incident flux,

$$\sigma[T_{wall}(t)]^4 = \alpha(t)\, \sigma[T_{rad}(t)]^4. \quad (2)$$

For our conditions, we calculate with LASNEX a maximum albedo of $\alpha \approx 0.8$, resulting in a correction of 11 eV at the peak of the x-ray drive. Figure 7b, which shows the hohlraum radiation temperature as a function of time from the PCD, indicates the validity of this approach.

For both types of experiments, we find smaller temperatures for $t > t_0 + 2$ ns than the values calculated with LASNEX. It is plausible that the effects of diagnostic hole closure start to become important at that time because the laser power is decreasing, and calculations show that cold blowoff plasma from the walls starts to move into the line of sight of the detector. More recently, we began working on a detailed experimental verification of the calculated, averaged charge number $Z$ of the gold plasma. The charge number is an important parameter in calculations of radiation production. Testing the calculations might help us to understand the observed discrepancy at late times in that a possible overestimation of $Z$ at late times will result in an overestimation of the radiation temperature as well.

When comparing the scattering losses for both types of experiments at different laser power (Figures 6b and 7c), we find that SBS losses increase significantly when increasing the laser power from PS22 to PS26. On the other hand, the losses by SRS are constant at approximately 1% of the incident laser energy. The SRS result

can be explained because the optical measurements for PS26 show narrow SRS spectra and no obvious beam deflection, very similar to the PS22 experiments described above. Figure 8 compares scattering losses observed with PS22 and PS26 for the various experiments. The increase of SBS losses with increasing laser power is not yet understood. The increase could be due to larger gain for the higher intensities encountered with PS26, or to the (spatial) laser amplitude modulations at the high fluences. Calculations are presently being performed to resolve this issue. Although most of the losses for PS26 occur after the maximum laser intensity, so that peak radiation temperatures are not affected, apparently SSD must be applied to reduce the scattering losses to acceptable small levels (5 to 10%).

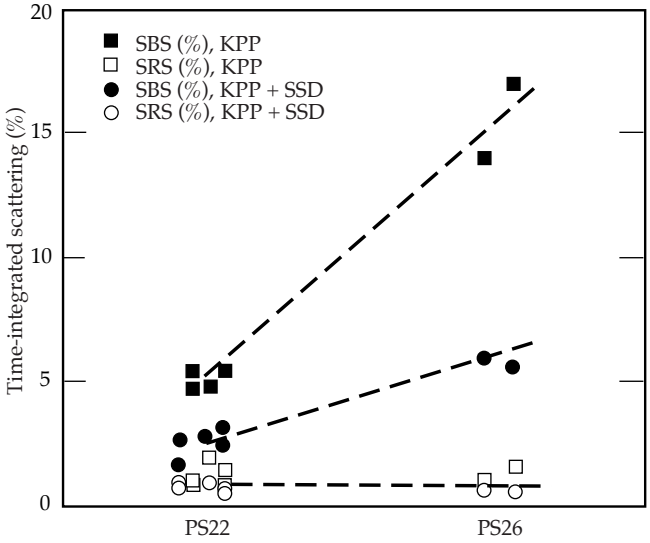


FIGURE 8. Comparison of total SBS and SRS losses for PS22 and PS26 in gas-filled hohlraums. The increase of the losses for PS26 could be related to higher gains or to laser amplitude modulations. (08-00-0598-1193pb01)

Figure 9 is a summary of the experimental hohlraum radiation temperatures obtained with varying (absorbed) laser power. The peak temperatures agree, within a standard deviation of 4 eV, with LASNEX modeling. The experimental peak radiation temperatures (after albedo correction) are plotted as a function of the laser power integrated over the high-intensity part of the laser drive 0.8 ns < $t$ < 1.8 ns (see Figures 6b and 7c). For gas-filled hohlraums, we achieve peak radiation temperatures of 215 eV for PS22, and 232 eV for PS26. The data is compared to detailed LASNEX calculations and to the results of the Marshak scaling for ablative heat waves[3,4]

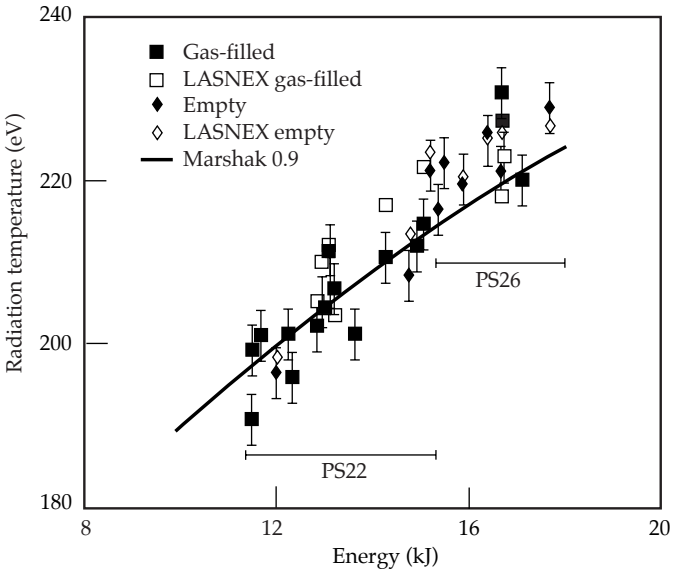


FIGURE 9. Experimental peak radiation temperatures of gas-filled and empty hohlraums for experiments with varying absorbed laser power during the high-intensity part of the pulse. The error of the individual data points is estimated to be 4 eV. Detailed LASNEX calculations agree with the experiments to within a standard deviation of 4 eV. Both the experiments and the calculations follow the scaling from Reference 13. (08-00-0598-1194pb01)

$$\eta P = AS_a + (A_{hole} + A_{cap})S_r . \quad (3)$$

This relation equates the power of the laser beams $P$ with the absorbed flux $S_a$ in the hohlraum wall of area $A$ and the reradiated flux $S_r$ through holes (area $A_{hole}$) or on the capsule (area $A_{cap}$). For Figure 4, we used constants from Reference 13 and a laser conversion of $\eta = 0.90$. The laser pulse was integrated only over the high-power part (0.8 to 1.8 ns), therefore neglecting the contribution of the low-power foot to the radiation temperature. This simplified model compares well to a more detailed scaling developed in Reference 35, which includes the foot contribution and results in $\eta = 0.85$. These values are in reasonable agreement with LASNEX simulations, which result in $\eta = 0.8$ to 0.9 (Ref. 12). The radiation temperatures of both the gas-filled and empty hohlraums compare well with each other and follow the scaling.

# Conclusions

We have demonstrated effective coupling of laser power in gas-filled inertial confinement fusion hohlraums by controlling and reducing laser scattering losses with laser beam smoothing techniques. This is an important result for present target designs of future ignition experiments, e.g., at the NIF. For the large-scale-length hohlraums of the NIF, calculations show that a symmetric high-yield capsule implosion

can be achieved when filling the hohlraum with a low-$Z$ gas to reduce the inward motion of the Au blowoff plasma from the hohlraum walls. We expect laser backscattering losses, which are caused by the addition of the gas, to be reduced when using laser beam smoothing with KPPs and by spectral dispersion. These techniques were included in the NIF design. Future experiments at Nova will test the specific SSD design that will be used in the NIF. It will also be important to extend the laser backscattering measurements of this study by using an $f/8$ focusing lens, which will be used at the NIF, and by testing other laser beam smoothing techniques, such as polarization smoothing, that might further reduce backscattering losses. In addition to new experiments, we are working on a more detailed comparison of the trends observed in the scattering measurements with calculations using the laser–plasma interaction code F3D.

The beneficial effects of the laser beam smoothing techniques were clearly seen in the radiation-temperature measurements of this study. We showed that radiation temperatures of both gas-filled and empty scale-1 hohlraums increase with KPP and KPP plus SSD and exceed 230 eV. They are reasonably well described by radiation hydrodynamic (LASNEX) modeling and scalings. The peak temperatures agree with the modeling, with a standard deviation of 4 eV, thus increasing our confidence in calculations for future inertial confinement fusion experiments.

## Acknowledgments

We thank R. W. Lee for helpful criticism. The support of the crew of the Nova laser facility and of M. Rushford is greatly appreciated.

## References

1. J. H. Nuckolls, *Phys. Today* **35** (9), 24 (1982).
2. J. D. Lindl, *Phys. Plasmas* **2**, 3933 (1995).
3. R. E. Marshak, *Phys. Fluids* **1**, 24 (1958).
4. R. Sigel et al., *Phys. Rev. Lett.* **65**, 587 (1990).
5. H. Nishimura et al., *Phys. Rev. A* **44**, 8323 (1991).
6. R. L. Kauffman et al., *Phys. Rev. Lett.* **73**, 2320 (1994).
7. S. W. Haan et al., *Phys. Plasmas* **2**, 2480 (1995).
8. W. J. Krauser, *Phys. Plasmas* **3**, 2084 (1996).
9. W. L. Kruer, *The Physics of Laser Plasma Interactions* (Addison-Wesley, New York, 1988).
10. T. P. Hughes, *Plasmas and Laser Light* (John Wiley and Sons, New York, 1975).
11. G. B. Zimmerman and W. L. Kruer, *Comments Plasma Phys. Controlled Fusion* **2**, 85 (1975).
12. L. J. Suter et al., *Phys. Rev. Lett.* **73**, 2328 (1994); L. J. Suter et al., *Phys. Plasmas* **3**, 2057 (1996).
13. R. Sigel et al., *Phys. Rev. A* **38**, 5779 (1988).
14. E. M. Campbell et al., *Rev. Sci. Intrum.* **57**, 2101 (1986).
15. B. A. Hammel et al., *Phys. Rev. Lett.* **70**, 1263 (1993).
16. M. D. Cable et al., *Phys. Rev. Lett.* **73**, 2316 (1994).
17. A. A. Hauer et al., *Phys. Plasmas* **2**, 2488 (1995).
18. N. D. Delamater et al., *Phys. Plasmas* **3**, 2022 (1996).
19. S. H. Glenzer et al., *Phys. Rev. Lett.* **79**, 1277 (1997).
20. S. N. Dixit et al., *Optics Lett.* **21**, 1715 (1996).
21. Y. Kato et al., *Phys. Rev. Lett.* **53**, 1057 (1985); D. M. Pennington et al., *Proc. SPIE* **1870**, 175 (1993).
22. R. H. Lehmberg and S. P. Obenschein, *Opt. Commun.* **46**, 27 (1983); S. Skupsky et al., *J. Appl. Phys.* **66**, 3456 (1989).
23. H. Kornblum et al., *Rev. Sci. Instrum.* **57**, 2179 (1986).
24. D. R. Kania et al., *Rev. Sci. Instrum.* **61**, 2765 (1990); L. S. Pan et al., *Appl. Phys. Lett.* **57**, 623 (1990).
25. C. Decker et al., *Phys. Rev. Lett.* 79, 1491 (1997).
26. B. J. MacGowan et al., *Phys. Plasmas* **3**, 2029, (1996).
27. R. K. Kirkwood et al., *Rev. Sci. Instrum.* **68**, 636 (1997).
28. H. S. Rose, *Phys. Plasmas* **3**, 1709 (1996).
29. J. D. Moody et al., *Phys. Rev. Lett.* **77**, 1294 (1996).
30. E. M. Epperlein and R. Short, *Phys. Fluids B* **4**, 2211 (1992).
31. R. L. Berger et al., *Phys. Fluids B* **5**, 2243 (1993).
32. V. Yu. Bychenkov et al., *Phys. Rev. E* **52**, 6759,(1995).
33. R. L. Kauffman et al., *Phys. Plasmas* **5**, 1927 (1998).
34. D. S. Hinkel et al., *Phys. Rev. Lett.* **77**, 1298 (1996).
35. E. Dattolo, H. Dumont, Y. Saillard, and J.-P. Jadaud, private communication (1995).